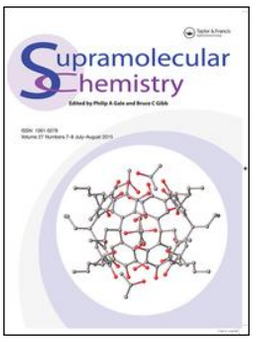

Supramolecular Chemistry

ISSN: 1061-0278 (Print) 1029-0478 (Online) Journal homepage: http://www.tandfonline.com/loi/gsch20

Luminescent sensing of Fe^{3+} and K^{+} by three novel imidazole dicarboxylate-based MOFs

Qiuying Huang, Jifeng Wang, Qi Wang & Gang Li

To cite this article: Qiuying Huang, Jifeng Wang, Qi Wang & Gang Li (2016): Luminescent sensing of Fe^{3+} and K^{+} by three novel imidazole dicarboxylate-based MOFs, Supramolecular Chemistry, DOI: 10.1080/10610278.2016.1198485

To link to this article: http://dx.doi.org/10.1080/10610278.2016.1198485

SUPRAMOLECULAR CHEMISTRY, 2016
http://dx.doi.org/10.1080/10610278.2016.1198485

Taylor & Francis
Taylor & Francis Group

Luminescent sensing of Fe^{3+} and K^+ by three novel imidazole dicarboxylate-based MOFs

Qiuying Huang[a], Jifeng Wang[b], Qi Wang[b] and Gang Li[b]

[a]Department of Chemical Engineering, Henan Polytechnic Institute, Nanyang, P.R. China; [b]College of Chemistry and Molecular Engineering, Zhengzhou University, Zhengzhou, P.R. China

ABSTRACT

In this paper, three luminescent metal–organic frameworks, namely: $[Zn(p\text{-IPhHIDC})]_n$ (**1**), $\{[Cd(p\text{-IPhIDC})(H_2O)]\cdot CH_3OH\}_n$ (**2**) and $[Zn(p\text{-TIPhHIDC})]_n$ (**3**), bearing two novel substituted imidazole dicarboxylate ligands, 2-(*p*-N-imidazol-1-yl)-phenyl-1*H*-imidazole-4,5dicarboxylic acid (*p*-$IPhH_3IDC$) and 2-*p*-(1H-1,2,4-triazol-1-yl)-phenyl-1*H*-imidazole-4,5dicarboxylic acid (*p*-$TIPhH_3IDC$), have been prepared and characterised through infrared spectra, X-ray powder diffraction, elemental analyses, thermogravimetric analyses and single-crystal X-ray diffraction. Ignoring the free methanol molecule and coordinated water in **2**, **1**–**3** are similar structures. Moreover, the luminescent properties of the MOFs have been explored. It was found that MOFs **1** and **2** show good luminescent sensing of Fe^{3+} in varying degrees, and **3** of K^+.

ARTICLE HISTORY
Received 1 May 2016
Accepted 1 June 2016

KEYWORDS
MOFs; substituted imidazole dicarboxylate; crystal structure; sensing property

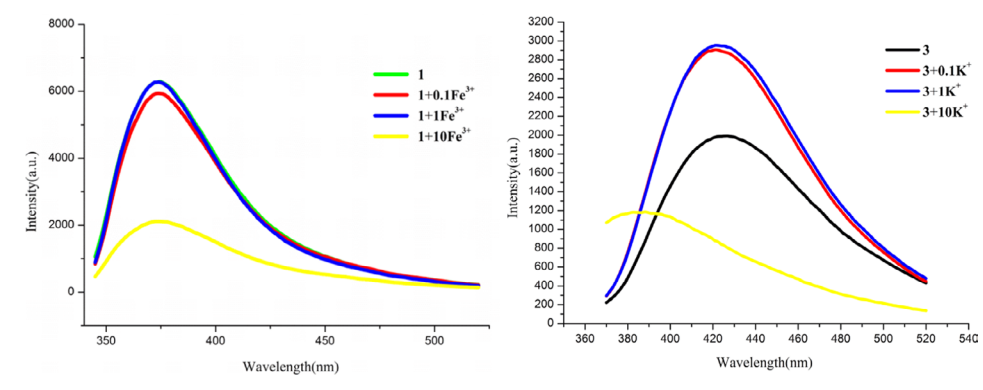

Two imidazole dicarboxylate-based ligands, 2-(*p*-N-imidazol-1-yl)-phenyl-1*H*-imidazole-4,5dicarboxylic acid and 2-*p*-(1H-1,2,4-triazol-1-yl)-phenyl-1*H*-imidazole-4,5dicarboxylic acid, and three corresponding luminescent MOFs have been prepared and characterised. The luminescent properties of the polymers have been explored. It was found that polymers **1** and **2** showed good uminescent sensing for Fe^{3+} in varying degrees, and **3** for K^+.

1. Introduction

Over the past three decades, the research community has witnessed the prominent growth of a special class of materials, namely: metal–organic frameworks (MOFs), that have risen to the forefront of solid-state chemistry. On account of their porosity, large specific surface area, unsaturated coordination position and diverse structures etc., MOFs are widely used in many fields, such as catalysis, gas storage/adsorption, optical, electric and magnetic materials, ion exchange and molecular recognition and so on (*1–12*). However, it is still a challenge to prepare more intriguing MOFs with various potential applications from designed multifunctional organic ligands. Consequently, considerable efforts have been devoted to design or choose the multifunctional bridging ligands.

In this context, due to the strong coordination ability and various coordination modes of two carboxylate groups and a imidazole ring (*13–16*), imidazole-4,5-dicarboxylic

CONTACT Gang Li gangli@zzu.edu.cn

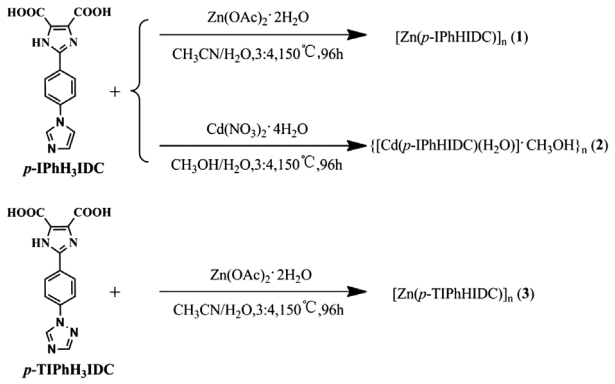

Scheme 1. Syntheses of MOFs **1–3**.

acid (H_3IDC) and its derivatives have attracted much attention. Several H_3IDC derivatives bearing aromatic groups at the 2-position of the imidazole ring and the related MOFs have been explored by our laboratory (*17–22*). The studies show that these substituted phenyl imidazole dicarboxylate ligands can build up interesting MOFs. Prompted by the findings, we continue to probe the substituent effect of the N-heterocycles on phenyl imidazole dicarboxylate ligands.

In this work, two novel organic ligands, 2-(*p*-N-imidazol-1-yl)-phenyl-1*H*-imidazole-4,5dicarboxylic acid (*p*-IPhH$_3$IDC) and 2-*p*-(1H-1,2,4-triazol-1-yl)-phenyl-1*H*-imidazole-4,5dicarboxylic acid (*p*-TIPhH$_3$IDC), bearing *N*-imidazol-1-yl or 1*H*-1,2,4-triazol-1-yl rings have been designed and prepared. Consequently, three related MOFs, [Zn(*p*-IPhHIDC)]$_n$ (**1**), {[Cd(*p*-IPhIDC)(H$_2$O)]·CH$_3$OH}$_n$ (**2**) and [Zn(*p*-TIPhHIDC)]$_n$ (**3**), have been constructed and structurally characterised (Scheme 1). Furthermore, the thermal and luminescent properties have been also investigated. To our surprise, in varying degrees, the three MOFs show a good luminescent sensing of Fe^{3+} or K^+, respectively. Although several examples of imidazole dicarboxylate-based complexes as anion or cation sensors have been previously reported (*23–25*), MOFs that sense K^+ have yet to be described.

2. Experimental section

2.1. Materials and methods

All chemicals were of reagent grade quality obtained from commercial sources and used without further purification.

The C, H and N analyses were carried out on a FLASH EA 1112 analyzer (Thermo Electron Corporation, Madison, WI, USA). IR spectra were recorded on a BRUKERTENSOR 27 spectrophotometer as KBr pellets in the 400–4000 cm^{-1} region (GMI, Inc., Ramsey, MN, USA). Thermogravimetric (TG) measurements were performed by heating the crystalline samples from 20 to 850 °C at a rate of 10°Cmin^{-1} in air on a Netzsch STA 409PC differential thermal analyzer (Germany NETZSCH Co. Selb, Germany). X-ray powder diffraction (XRD) measurements were recorded on a Panalytical X'pert PRO X-ray diffractometer (PANalytical B.V. Holland). Fluorescence spectra were characterised at room temperature by a F-4600 fluorescence spectrophotometer (Hitachi High-Technologies Co. Tokyo, Japan) (240 nm/min). UV–visible absorption spectra were measured on a Agilent 8453 spectrophotometer (Agilent Technologies, USA). The ^{1}H-NMR spectra were recorded at ambient temperature using a Bruker DPX 400 instrument and were referenced internally to residual solvent resonances (Bruker instrument Co., Germany).

2.2. Preparation of the organic ligands, p-IPhH$_3$IDC and p-TIPhH$_3$IDC

As shown in Scheme 2, 2, 3-bis(nitrooxy)maleic acid, 4-(1*H*-imidazol-1-yl)benzaldehyde and 4-(1*H*-1,2,4-triazol-1-yl)benzaldehyde were firstly prepared by us, and then organic ligands, *p*-IPhH$_3$IDC and *p*-TIPhH$_3$IDC, were made according to the literature procedure (*26*). Anal. Calcd. for *p*-IPhH$_3$IDC: C, 56.38; H, 3.38; N, 18,79%; Found: C, 56.52; H, 3.26; N, 19.02%. IR (cm^{-1}, KBr): 3484 (m), 3116 (w), 2939 (w), 2704(w), 1934 (m), 1725 (w), 1536 (m), 1419 (s), 1356 (s), 1274 (w), 1124 (s), 1052 (s), 956 (s), 842(s), 771 (w), 734 (s), 699 (s), 649 (s), 622(w), 563 (w). ^{1}H NMR (300 MHz, DMSO, 25°C, TMS, ppm): 9.61 (s, 1H, –NH), 9.01 (d, 2H, –C$_5$H$_3$N$_2$), 8.41 (d, 1H, –C$_5$H$_3$N$_2$), 8.39 (d, 2H, –C$_6$H$_4$), 8.31–8.33 (d, 2H, –C$_6$H$_4$). UV-vis (CH$_3$CN): 635 nm (m), 649 nm (w). Anal. Calcd for *p*-TIPhH$_3$IDC: C, 52.18; H, 3.04; N, 23.41%; Found: C, 52.37; H, 3.34; N, 23.75%. IR (cm^{-1}, KBr): 3407 (m), 3115 (w), 2748 (w), 2568(w), 1934 (m), 1724 (m), 1511 (m), 1359 (s), 1278 (s), 1214 (w), 1141 (s), 1039 (s), 967 (w), 842 (s), 796 (s), 771 (s), 736 (s), 696(w), 669 (w). ^{1}H NMR (300 MHz, DMSO, 25°C, TMS, ppm): 9.45 (s, 1H, –NH), 9.11 (d, 1H, –C$_5$H$_3$N$_2$), 8.46 (d, 1H, –C$_5$H$_3$N$_2$), 8.38 (d, 2H, –C$_6$H$_4$), 8.30–8.32 (d, 2H, –C$_6$H$_4$).UV-vis (CH$_3$CN): 639 nm (m), 651 nm (w).

2.3. Preparation of crystalline polymer [Zn(p-IPhHIDC)]$_n$ (1)

A mixture of Zn(OAc)$_2$·2H$_2$O (21.9 mg, 0.1 mmol), *p*-IPhH$_3$IDC (29.8 mg, 0.1 mmol), H$_2$O-CH$_3$CN (4:3, 7 mL) and hydrochloric acid (0.05 mL, 36–38%) was sealed in a 25-mL Teflon-lined bomb and heated at 150(C for 96 h, and then allowed to cool to room temperature. The brown acicular crystals of **1** were collected, washed with distilled water and dried in air (72% yield based on Zn). Anal. Calcd for C$_{14}$H$_8$N$_4$O$_4$Zn: C, 46.50; H, 2.23; N, 15.50%; Found: C, 46.32; H, 2.14; N, 15.85%. IR (cm^{-1}, KBr): 3424(m), 3234(w), 3098(m), 2171(s), 1959(w), 1722(s), 1531(w), 1506(w), 1377(s), 1132(w), 1068(s), 856(m), 739(m), 659(m), 572(m).

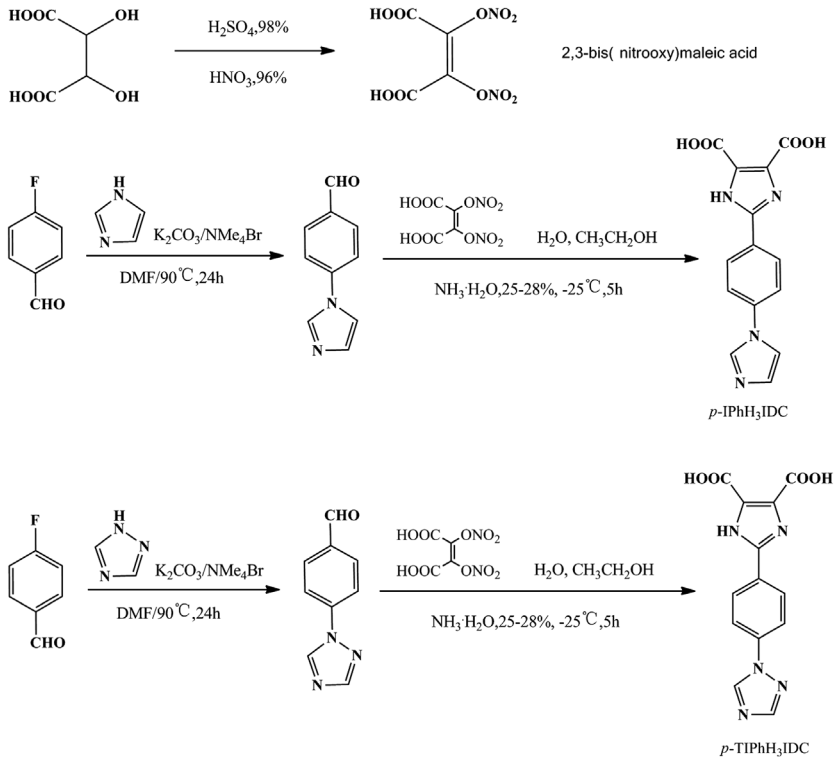

Scheme 2. Synthesis pathways of the organic ligands.

2.4. Preparation of crystalline polymer {[Cd(p-IPhHIDC)(H_2O)]·CH_3OH}$_n$ (2)

Polymer **2** was prepared in a manner analogous to that used to prepare **1,** only $Cd(NO_3)_2{\cdot}4H_2O$ (30.8 mg, 0.1 mmol) was used instead of $Zn(OAc)_2{\cdot}2H_2O$ and H_2SO_4 (0.05 mL, 36–38%). The colourless crystals of two were isolated, washed with distilled water and dried in air (54.5% yield based on Cd). Anal. Calcd. for$C_{15}H_{14}N_4O_6Cd$: C, 39.27; H, 3.08; N, 12.22%; Found: C, 39.20; H, 2.71; N, 12.14%. IR (cm^{-1}, KBr): 3425 (s), 3115 (m), 2170 (s), 1895 (m), 1682 (s), 1529 (m), 1386 (m), 1268 (w), 1061 (m), 847 (m), 749 (s), 732 (s), 511 (m).

2.5. Preparation of crystalline polymer [Zn(p-TIPhHIDC)]$_n$ (3)

A mixture of $Zn(OAc)_2{\cdot}2H_2O$ (21.9 mg, 0.1 mmol), *p*-TIPh-H_3IDC (12.0 mg, 0.04 mmol), H_2O-CH_3CN (4:3, 7 mL) and hydrochloric acid (0.1 mL, 36–38%) was sealed in a 25-mL Teflon-lined bomb and heated at 150 °C for 96 h, then allowed to cool to room temperature. Then, the brown acicular crystals of **3** were collected, washed with distilled water and dried in air (55% yield based on Zn). Anal. Calcd. for $C_{13}H_7N_5O_4Zn$: C, 43.06; H, 1.95; N, 19.32%; Found: C, 42.75; H, 1.78; N, 18.97%. IR (cm^{-1}, KBr): 3442 (m), 3088 (w), 2920 (w), 2850 (s), 1578 (s), 1536 (s), 1469 (s), 1279 (s), 1288 (m), 1140 (m), 977 (w), 864 (m), 748 (m), 673 (w), 560 (w), 526 (w).

2.6. Crystal structure determinations

Suitable single crystals of compounds **1–3** were selected for single-crystal X-ray diffraction analyses. The intensity data were measured on a Bruker Smart 1000 diffractometer with a graphite-monochromated MoKα radiation (λ = 0.71073 Å). Single crystals of **1–3** were selected and mounted on a glass fibre. All data were collected at room temperature using the $\omega - 2\theta$ scan technique and corrected for Lorenz polarisation effects. A correction for secondary extinction was applied.

The three structures were solved by direct methods and expanded using the Fourier technique. The non-hydrogen atoms were refined with anisotropic thermal parameters. The hydrogen atoms on C were positioned geometrically and refined using a riding model. The hydrogen atoms on O were found at reasonable positions in the differential Fourier map and located there. All the hydrogen atoms were included in the final refinement. The final cycle of full-matrix least squares refinement was based on 2430 observed reflections and 208 variable parameters for **1**, 2870 observed reflections and 246 variable parameters for **2** and 2350 observed reflection and 208 variable parameters for **3**. All calculations were performed using the SHELX-97 crystallographic software package (*27*). The crystallographic data, and selected bond lengths and angles are given in Tables 1 and 2, respectively.

Table 1. Crystallographic data for polymers **1–3**.

	1	2	3
Formula	$C_{14}H_8N_4O_4Zn$	$C_{15}H_{14}N_4O_6Cd$	$C_{13}H_7N_5O_4Zn$
F_w	361.63	458.70	362.61
Crystal system	Monoclinic	Monoclinic	Monoclinic
Crystal size/mm	0.20 × 0.20 × 0.20	0.22 × 0.21 × 0.19	0.49 × 0.33 × 0.20
Space group	$P2_1/c$	$P2_1/n$	$P2_1/n$
a, Å	8.6321(6)	8.8099(4)	8.6757(6)
b, Å	13.0479(9)	15.3396(7)	12.6925(8)
c, Å	12.9456(9)	12.5757(6)	12.8642(9)
α, °	90	90	90
β °	108.5992(11)	105.342(5)	109.097(8)
γ,°	90	90	90
V, Å^3	1381.92(17)	1638.92(13)	1338.60(16)
Dc, Mg m^{-3}	1.738	1.859	1.799
Z	4	4	4
μ, mm^{-1}	1.805	1.375	1.865
ReflnscollectedIunique	7135/ 2430 [R(int) = 0.0208]	6306 / 2870 [R(int) = 0.0330]	5200 / 2350 [R(int) = 0.0292]
Data/restraints/parameters	2430 / 0 /208	2870 / 6 / 246	2350 / 0 / 208
R	0.0994	0.0385	0.0433
R_w	0.2533	0.0919	0.1179
GOF on F^2	1.215	1.012	1.042
$\Delta\rho_{max}$ and $\Delta\rho_{min}$, e Å^{-3}	0.693 and −1.354	1.113 and −0.693	0.517 and −0.530

Table 2. Selected bond distances (Å) and angles (deg) for complexes **1–3.**

1			
Zn(1)-N(3)#1	2.033(7)	Zn(1)-N(4)#2	2.158(7)
Zn(1)-O(4)	2.062(7)	N(4)-Zn(1)#3	2.158(7)
Zn(1)-O(2)	2.069(6)	N(3)-Zn(1)#4	2.033(7)
Zn(1)-N(2)	2.130(6)		
N(3)#1-Zn(1)-O(4)	129.4(3)	O(2)-Zn(1)-N(2)	81.2(2)
N(3)#1-Zn(1)-O(2)	115.8(3)	N(3)#1-Zn(1)-N(4)#2	91.5(3)
O(4)-Zn(1)-O(2)	114.5(3)	O(4)-Zn(1)-N(4)#2	80.3(3)
N(3)#1-Zn(1)-N(2)	96.2(3)	O(2)-Zn(1)-N(4)#2	93.7(3)
O(4)-Zn(1)-N(2)	96.1(3)	N(2)-Zn(1)-N(4)#2	172.1(3)
2			
Cd(1)-N(2)	2.248(4)	Cd(1)-O(1 W)	2.377(4)
Cd(1)-N(1)#1	2.257(4)	Cd(1)-O(1)#1	2.399(4)
Cd(1)-N(4)#2	2.289(4)	Cd(1)-O(4)	2.473(4)
Cd(1)#3-N(1)	2.257(4)	Cd(1)#3-O(1)	2.399(4)
Cd(1)#2-N(4)	2.289(4)		
N(1)#1-Cd(1)-O(1)#1	72.35(12)	N(4)#2-Cd(1)-O(1)#1	98.36(15)
N(2)-Cd(1)-N(1)#1	157.03(15)	O(1 W)-Cd(1)-O(1)#1	178.29(14)
N(2)-Cd(1)-N(4)#2	100.42(14)	N(2)-Cd(1)-O(4)	70.82(12)
N(1)#1-Cd(1)-N(4)#2	95.13(14)	N(1)#1-Cd(1)-O(4)	100.89(13)
N(2)-Cd(1)-O(1 W)	90.20(16)	N(4)#2-Cd(1)-O(4)	155.36(14)
N(1)#1-Cd(1)-O(1 W)	108.49(16)	O(1 W)-Cd(1)-O(4)	74.16(14)
N(4)#2-Cd(1)-O(1W)	83.09(16)	O(1)#1-Cd(1)-O(4)	104.26(14)
N(2)-Cd(1)-O(1)#1	88.64(13)		
3			
Zn(1)-O(4)#1	2.037(3)	Zn(1)-N(3)#1	2.135(3)
Zn(1)-N(5)#2	2.071(4)	N(3)-Zn(1)#3	2.135(3)
Zn(1)-O(1)	2.078(3)	N(5)-Zn(1)#4	2.071(4)
Zn(1)-N(1)	2.119(3)	O(4)-Zn(1)#3	2.037(3)
O(4)#1-Zn(1)-N(5)#2	128.21(13)	O(1)-Zn(1)-N(1)	80.48(11)
O(4)#1-Zn(1)-O(1)	114.21(14)	O(4)#1-Zn(1)-N(3)#1	81.11(11)
N(5)#2-Zn(1)-O(1)	117.10(13)	N(5)#2-Zn(1)-N(3)#1	89.98(13)
O(4)#1-Zn(1)-N(1)	99.30(11)	O(1)-Zn(1)-N(3)#1	92.67(12)
N(5)#2-Zn(1)-N(1)	95.40(14)	N(1)-Zn(1)-N(3)#1	172.69(12)

Note. Symmetry codes for **1**: #1: *–x* + 1, *y* + 1/2, -*z* + 1/2; #2: *x*, *–y* + 1/2, *z* + 1/2; #3: *x*, *–y* + 1/2, *z*–1/2; #4: *–x* + 1, *y*–1/2, *–z* + 1/2; For **2**: #1: *x*–1/2, *–y* + 1/2, *z*–1/2; #2: *–x*, *–y* + 1, *–z* + 1; #3: *x* + 1/2, *–y* + 1/2, *z* + 1/2; For **3**: #1: *x*–1/2, *–y* + 1/2, *z*–1/2; #2: *–x* + 1/2, *y*–1/2, *–z* + ½; #3: *x* + 1/2, *–y* + 1/2, *z* + ½; #4: *–x* + 1/2, *y* + 1/2, *–z* + 1/2.

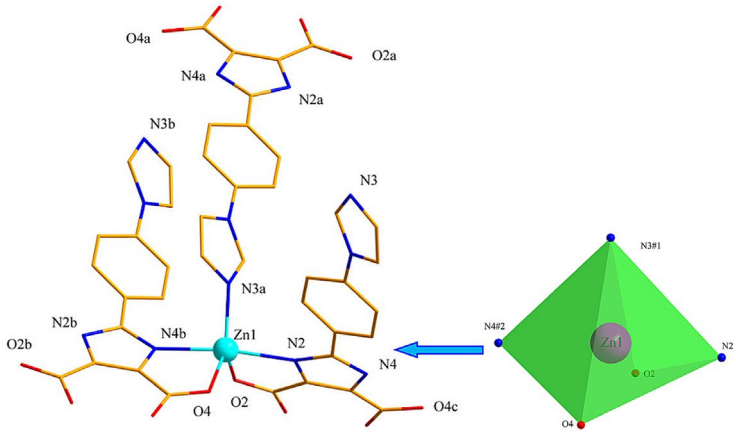

(a)

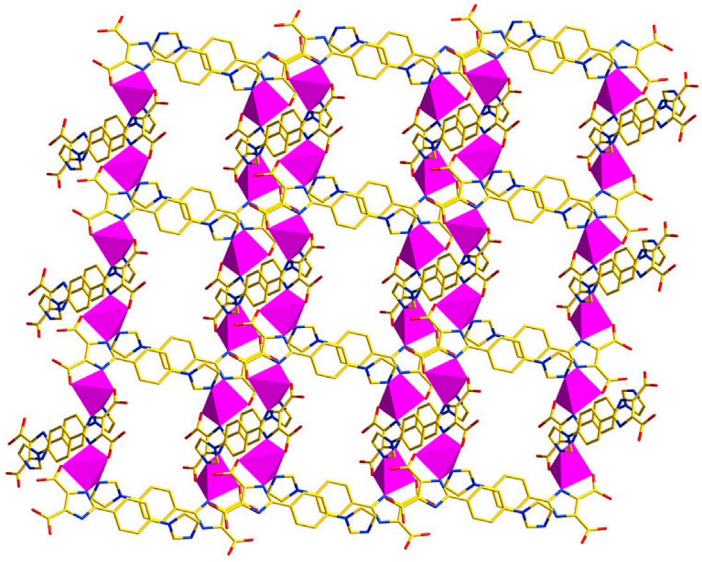

(b)

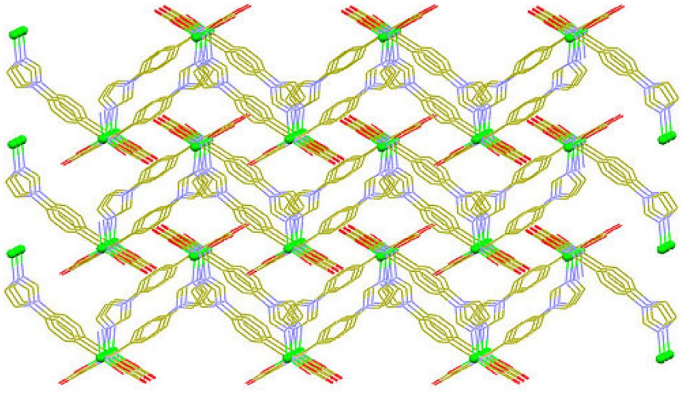

(c)

Figure 1. (Colour online) (a) Coordination environment of Zn^{2+} atom in **1** (H atoms omitted for clarity). (b) 2D layer of **1**. (c) The 3D solid-state framework of **1** constructed by π...π Interaction.

2.7. Luminescence experiments

Luminescent properties of 1 (or 2 or 3)/M^{n+} (n = 1 or 2 or 3) were investigated in the solid state at room temperature. The 1 (or 2 or 3)/M^{n+} (n = 1 or 2 or 3) samples were prepared by introducing 80 mg of 1 (or 2 or 3) crystalline powder into 4.0 mL of different aqueous solutions of $M(NO_3)_x$

(0.01 mol/L) (M = Na^+, K^+, Mg^{2+}, Ca^{2+}, Al^{3+}, Fe^{3+}, Co^{2+}, Ni^{2+}, or Pb^{2+}, et al.), and treated for 17 h; then, the powder was isolated and washed with redistilled water, and dried in air for fluorescence study.

3. Results and discussion

3.1. Crystal structures of crystalline polymers

The crystal structures of polymers **1**–**3** are similar, ignoring the free methanol molecule and coordinated water in **2**. That is to say, they have the same topology structures. Therefore, we will restrict our description to the polymer **1**, and only mention pertinent points for the polymers **2** and **3**, where appropriate.

Polymer **1** crystallises in monoclinic space group $P2_1/c$. The asymmetric unit of **1** comprises one metal centre and three *p*-IPhHIDC^{2-} ligands (Figure 1a). The Zn^{2+} is penta-coordinated with three N and two O atoms forming a twisted double-tapered hexahedron, in which O2, N2 and O4, N4#2 are from two imidazole dicarboxylate ligands, respectively, and N3#1 atom is from the imidazole ring at the 4-position of benzene from another *p*-IPhHIDC^{2-} ligand. Zn–N bond lengths are in the range of 2.033(7)–2.033(7) Å. Zn–O distances vary from 2.062(7) to 2.069(6) Å. The bond angles around each Zn(II) are in the range of 80.3(3)–172.1(3)°, which are consistent with the values in literature (*28, 29*).

Each μ_3-*p*-IPhHIDC^{2-} anion connects the adjacent Zn(II) atoms through N,O-chelating or N′,O′-chelating modes to form a one-dimensional chain along the *c*-axis (Figure 1b). The chains are bridged by the μ_3-*p*-IPhHIDC^{2-} anions and expanded into a layer structure. Furthermore, these layers are assembled into a three-dimensional supramolecular solid-state structure via *π*...*π* stacking interactions between the neighbouring two benzene rings (dihedral angle being 0.000° and distance being 3.2908 Å between the two benzene rings) (Figure 1c).

As shown in Figure 2a, for polymer **2**, the central Cd(II) ion is six-coordinated with three O and three N atoms, forming a distorted octahedron, in which O1 W is from the coordinated water, O1#1, N1#1, O4 and N2 atoms are from two *p*-IPhHIDC^{2-} ligands, respectively, and N4#2 is from the imidazole at the 4-position of benzene of another *p*-IPhHIDC^{2-} ligand. As indicated in Figure 2b and c, the structure of **2** is similar to that of **1**. The Cd–N and Cd–O lengths are in the range of 2.248(4)–2.289(4) Å and 2.377(4)–2.473(4) Å, respectively, which are in accordance with the values in previous documents (*28*). The bond angles around each Cd^{2+} ion vary from 70.82(12)° to 157.03(15)°.

As depicted in Figure 3, the coordination environment of each Zn^{2+} ion and the 3D solid-state framework of **3** are same to those of **1**. The Zn–N and Zn–O lengths range from 2.071(4) Å to 2.135(3) Å and from 2.037(3) Å to 2.078(3) Å, respectively. The bond angles around each Zn^{2+} ion vary from 80.48(11)° to 172.69(12)°, which are all similar to those reported in the literature (*28, 29*).

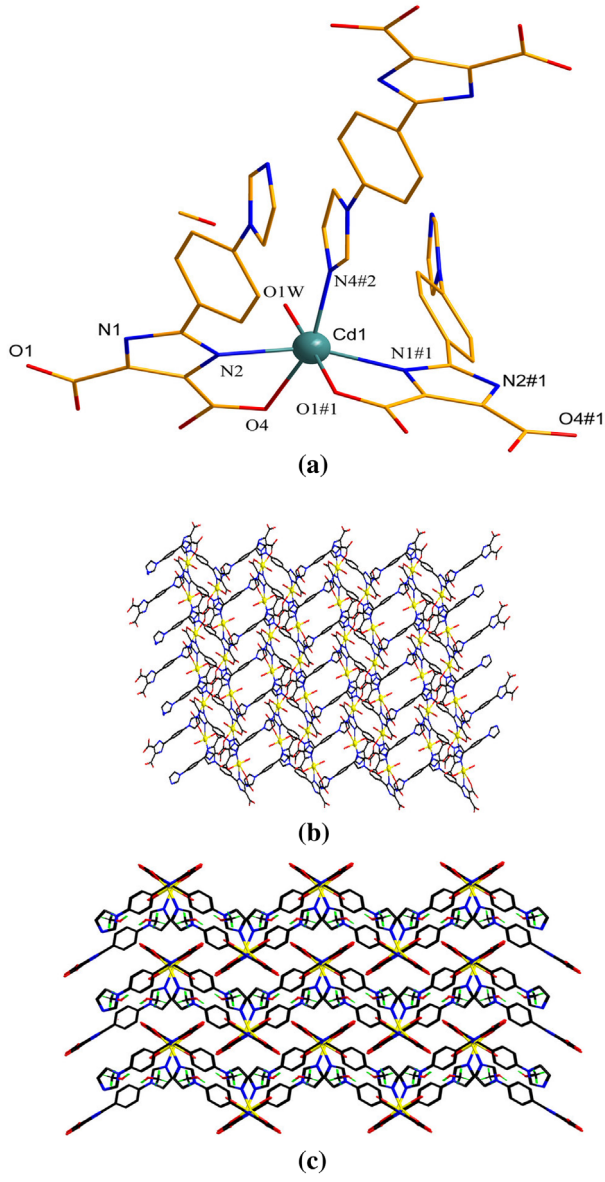

Figure 2. (Colour online) (a) Coordination environment of Cd^{2+} atom in **2** (partial H atoms are omitted for clarity). (b) The 2D sheet of **2**. (c) The 3D solid-state structure of **2** built by *π*...*π* Interaction. (B&W for printed version).

The *p*-IPhHIDC^{2-} and *p*-TIPhHIDC^{2-} ligands in **1–3** all adopt the same coordination mode, μ_3-*k*N, O; *k*N′, O′; *k*N″ (Scheme 3).

To understand the framework of **3** better, it is necessary to simplify the blinding blocks of compound **3**. Each imidazole dicarboxylate ligand connects three cations, which can be represented by a three-connected unit, and each cation bridges three imidazole dicarboxylate ligands and can be represented by the three-connected unit. Therefore, the whole structure can be simplified as a (2, 4)-connected net (Figure 3d).

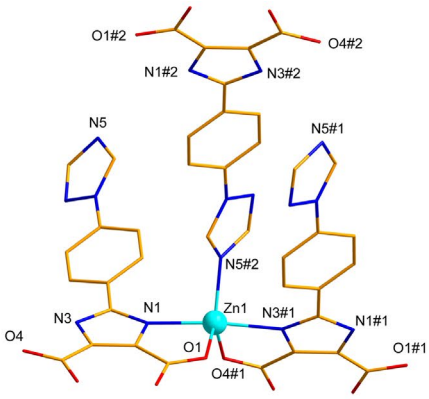

(a)

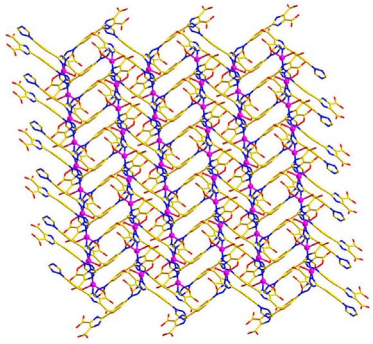

(b)

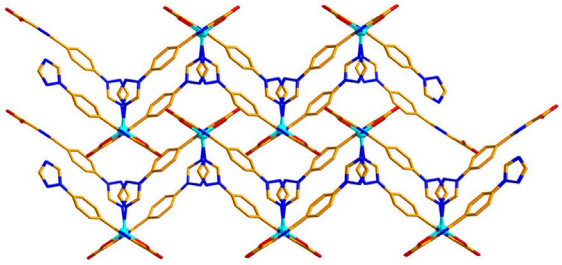

(c)

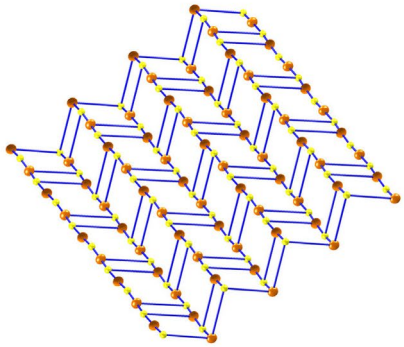

(d)

Figure 3. (Colour online) (a) Coordination environment of Zn^{2+} atom in **3** (H atoms omitted for clarity). (b) 2D sheet of **3**. (c) The 3D solid-state framework of **3** constructed by $\pi\ldots\pi$ Interaction. (d) The (3,3)-connected network of **1–3** by considering the organic ligand as a three-connected node and the cation as a three-connected node (For **2,** the free methanol molecule and the coordinated water are omitted). (B&W for printed version).

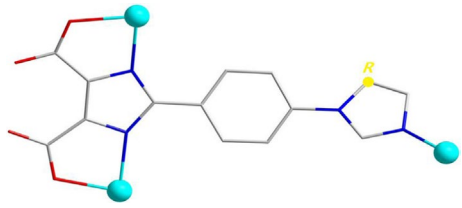

Scheme 3. (Colour online) Coordination modes of the imidazole dicarboxylate ligands (for *p*-IPhHIDC^{2-} R=C , for *p*-TIPhHIDC^{2-} R=N).

3.2. XRD Patterns and thermal analyses

To confirm the phase purity of the three polymers, the XRD patterns were recorded. Most of the peak positions of simulated and measured patterns are in good agreement with each other (Figure 4).

The thermogravimetric analyses of the three complexes were carried out to investigate the thermal stabilities within the range of 20.0–850 °C (Figure 5). As seen from the TG curves, polymers **1–3** are stable up to 330 °C. The whole weight losses are from 332 to 652 °C for **1**, from 326 to 639 °C for **2** and from 324 to 681 °C for **3**, which can be attributed to the decomposition of the collapse of organic ligands**.**

In conclusion, the thermal data of complexes **1**–**3** are in reasonable agreement with the crystal structure analyses.

3.3. Luminescence behaviours and sensing properties

MOFs have received much attention due to their potential applications in luminescene sensing for small molecules, ions and so on (*30–33*). Enlightened by such interesting luminescent properties of the MOFs, the solid-state fluorescent and sensing properties of **1–3** have been investigated at room temperature.

The luminescence spectra of the free organic ligands, *p*-IPhH_3IDC and (*p*-TIPhH_3IDC, and polymers were determined in solid state at room temperature (Figure 6). Compared with the free ligands, the emission peaks of the polymers **1–3** occur (blue shift) at varying degrees. As shown in figure 6a, the free *p*-IPhH_3IDC ligand displays luminescence, with the emission maximum at 479 nm by selective excitation at 410 nm which is attributed to the $\pi^*\rightarrow$n transition. Polymers **1** and **2** indicate relatively strong luminescence, with an emission maximum at 373 nm upon excitation at 275 nm for **1** and with an emission maximum at 429 nm upon excitation at 356 nm for **2**. They show blue shift (106 nm for **1**, 50 nm for **2**) compared with the emission spectrum of *p*-IPhH_3IDC. The free ligand *p*-TIPhH_3ID exhibits a strong emission at 493 nm when excited at 441 nm. The emission maximum peak of polymer **3** is at 429 nm excited at 356 nm, which

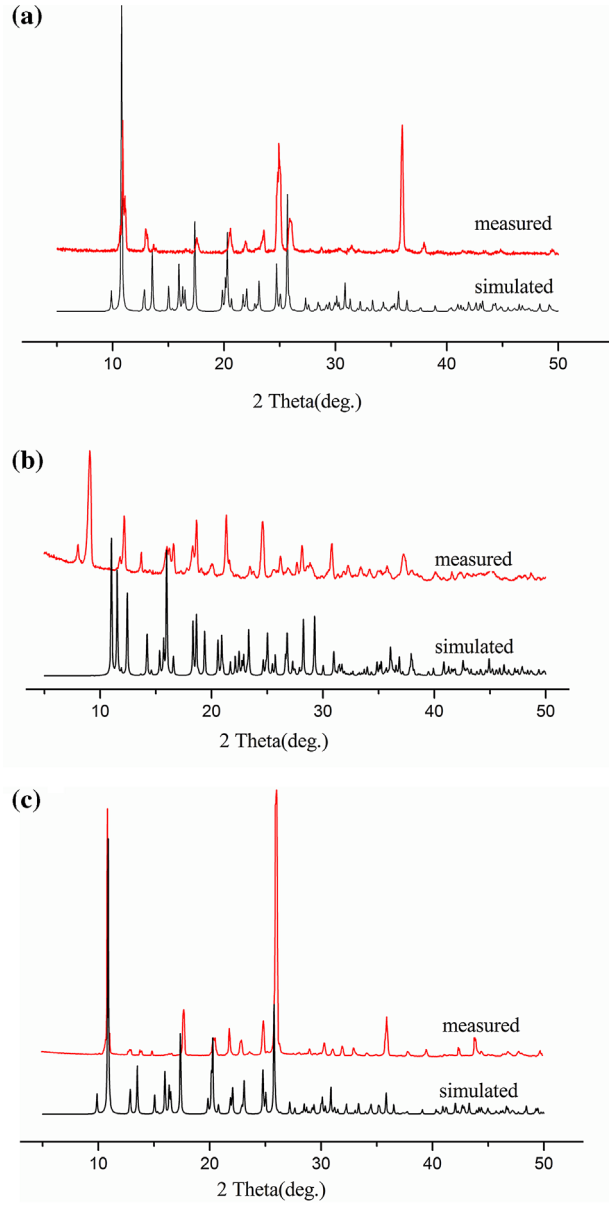

Figure 4. (Colour online) XRD spectra of polymers **1–3.**

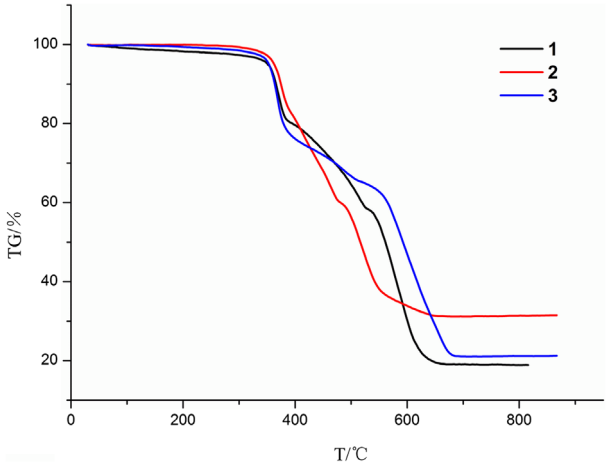

Figure 5. (Colour online) TG analysis profiles of polymers **1–3**.

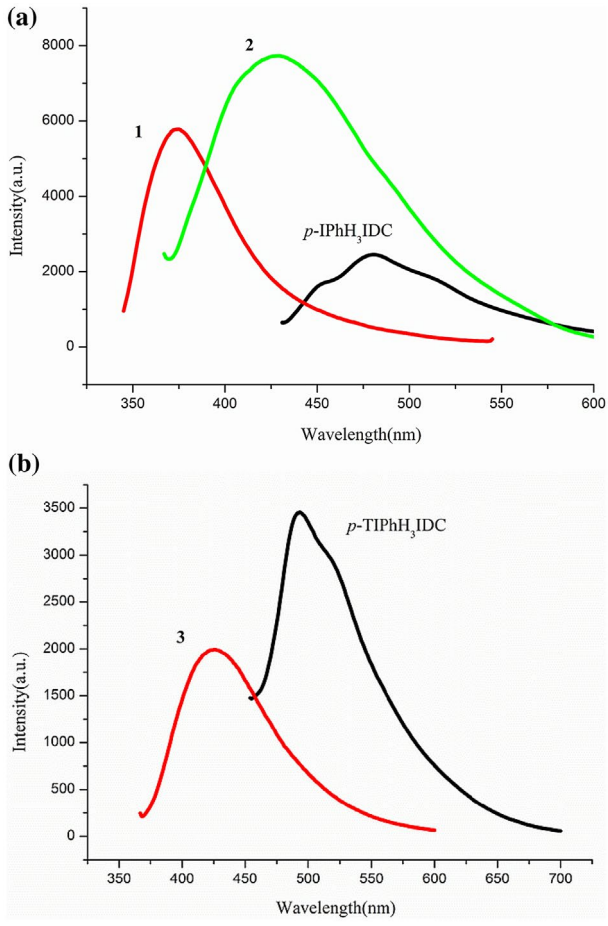

Figure 6. (Colour online) (a) PL intensity of the ligand *p*-IPhH$_3$ID and polymers **1–2**. (b) PL intensity of the ligand *p*-TIPhH$_3$ID and polymer **3**.

indicates 64-nm blue shift compared with the free ligand *p*-TIPhH$_3$ID (Figure 6b).

Since the Zn(II) and Cd(II) ions are difficult to oxidise or to reduce due to their features of electronic configurations, the emission bands of complexes of **1** and **2** are neither metal-to-ligand charge transfer (MLCT) nor ligand-to-metal charge transfer in nature. So the emission of **1** and **2** might be attributed to the ligand-to-ligand charge transfer, and the blue shift of **1–3** is due to intramolecular charge transfer (ICT).

The photoluminescence sensing experiments of polymer$_+$**M** are determined at room temperature (Figure 7). It is interesting to find that **1** and **2** show selective recognition for Fe^{3+} ion, and polymer **3** shows good sensing for K^+.

As shown in Figure 7a, it could be found that the luminescent intensity of **1** heavily depends on the type of metal ions: Co^{2+}, Ni^{2+} and Na^+ ions have basically no effect on its luminescence, while other cations have slight effects on the luminescent intensity (increasing (Sr^{2+} and K^+) or decreasing (Cd^{2+}, Mg^{2+}, Ca^{2+}, Pb^{2+} and Al^{3+}) effects). Impressively, the luminescent intensity is nearly one-third

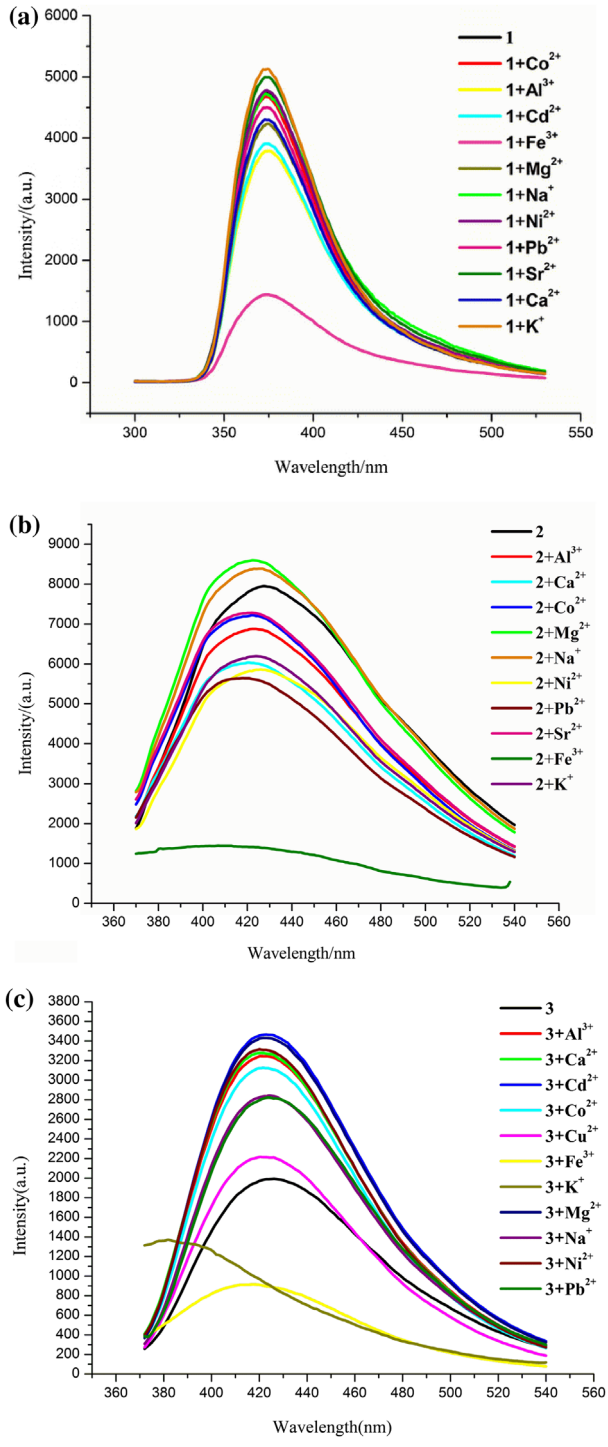

Figure 7. (Colour online) Photoluminescence intensity of polymers, **1**(a), **2**(b) and **3**(c) treated by different metal salt solutions.

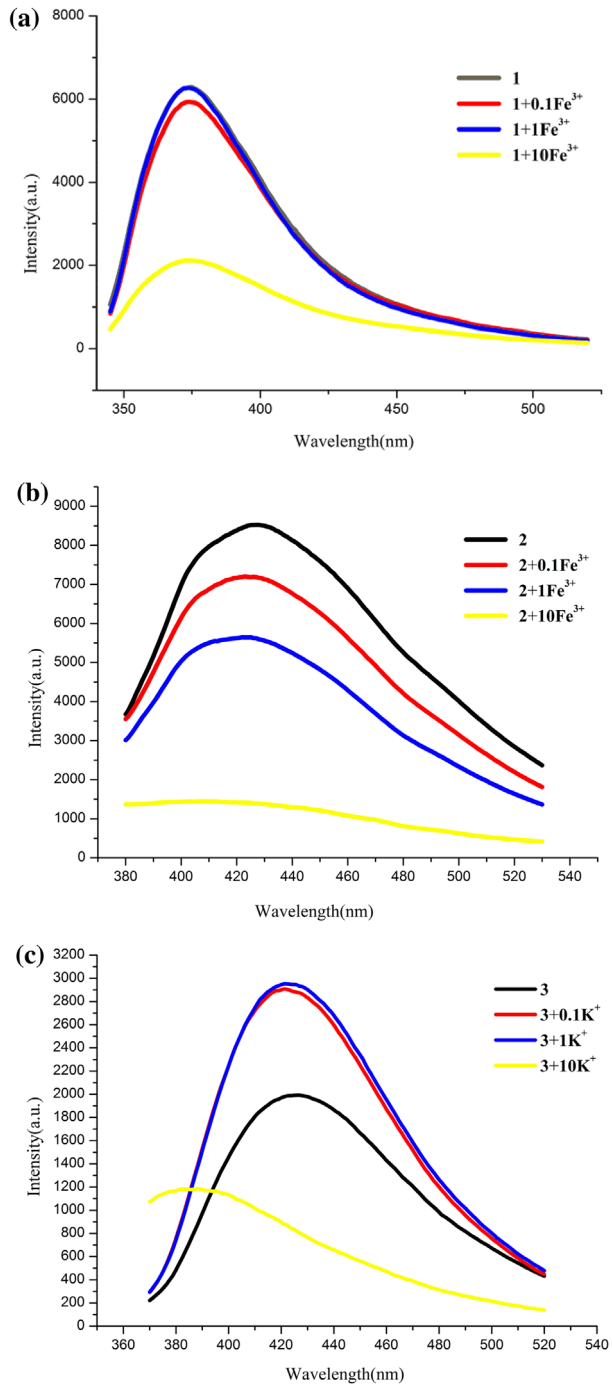

Figure 8. (Colour online) (a) Emissive response spectra of **1** treated by $Fe^{3+}$of different molar concentrations. (b) Emissive response spectra of **2** treated by Fe^{3+} of different molar concentrations. (c) Emissive response spectra of **3** treated by K^+ of different molar concentrations.

of **1** after treatment with Fe^{3+} ion. For polymer **2**, the most metal ions (Cd^{2+}, Mg^{2+}, Ca^{2+}, Pb^{2+}, Al^{3+}, Sr^{2+}, K^+, Co^{2+} and Ni^{2+}) have varying degrees on the luminescent intensity, but Fe^{3+} ion has a dramatic quenching effect (Figure 7b). As indicated in Figure 7c, both Fe^{3+} and K^+ ions have notable quenching effect. At the same time, there is an approximate 48-nm blue shift of the emission band induced by K^+ ion (λex = 274 nm) (Figure 7c). That is to say, the recognition effect of **3** for K^+ ion is more distinct.

To examine the sensing sensitivity towards Fe^{3+} or K^+ in more detail, the samples of compounds **1–3** treated by increasing Fe^{3+} or K^+ concentrations (0.1, 1, 10 mmol/L)

were prepared, and their emission spectra were recorded (Figure 8). As shown in Figure 8, it can be clearly seen that the fluorescence intensity gradually decreases with increase in Fe^{3+} or K^{+} contents, which indicates that **1** and **2** are promising fluorescent probes for detecting Fe^{3+} cation, and **3** for K^{+}.

To elucidate the possible mechanism for such luminescence behaviours, as well as to identify if the frameworks of **1–3** collapse after treatment with different metal ions, the XRD and IR spectra (Figure 9) of the solid-state samples were carried out. XRD data showed that the as-synthesised products are in good agreement with the corresponding simulated ones, indicating the phase purity of the samples. In addition, the results of XRD and IR spectra indicate no obvious difference in **1** (or **2** or **3**) immersing in different cation solutions before or after, revealing that the original framework remains upon treatment. So, the introduction

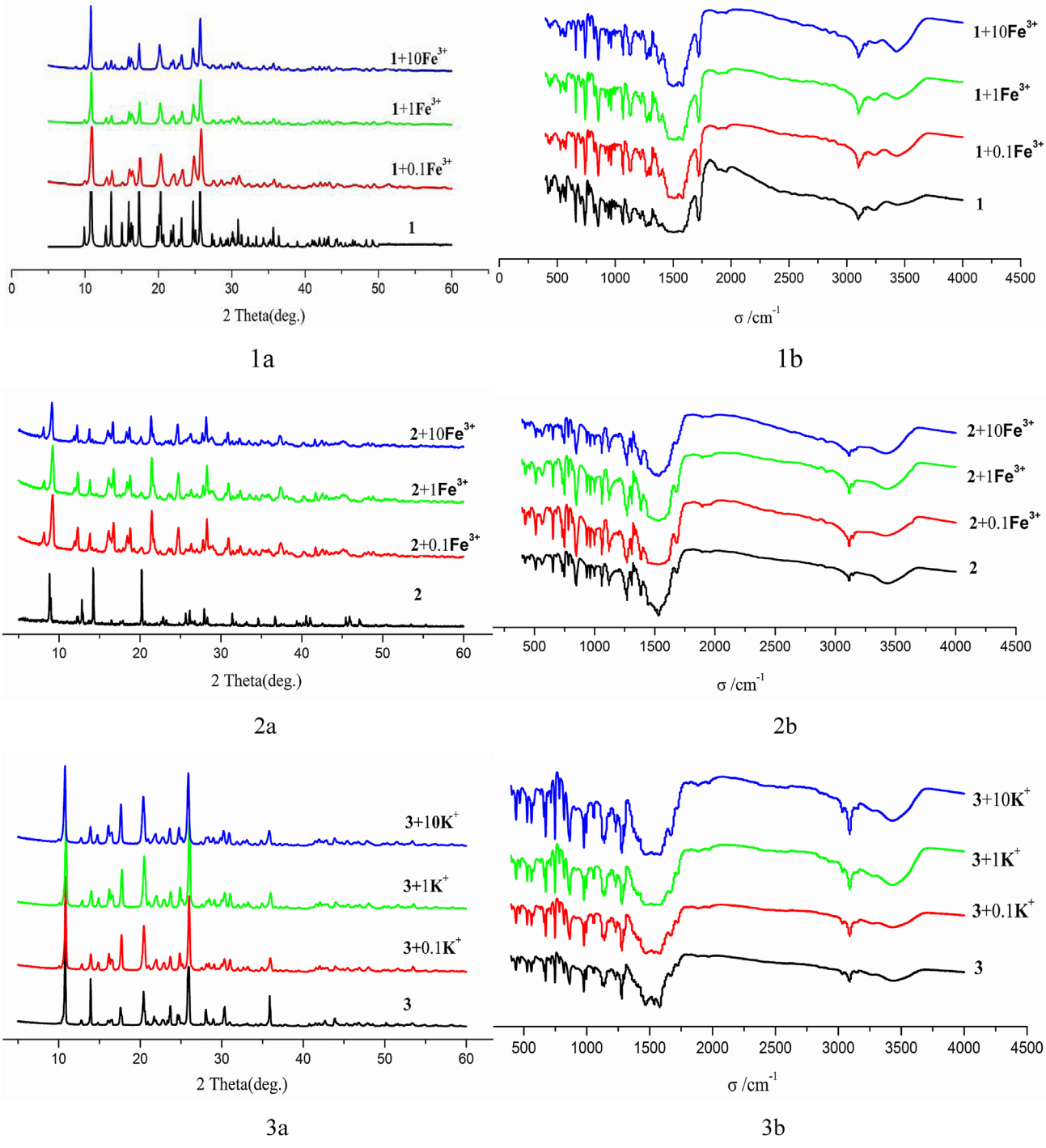

Figure 9. (Colour online) XRD (a) and IR (b) spectra of the polymers treated by different concentrations of metal salt aqueous solution.

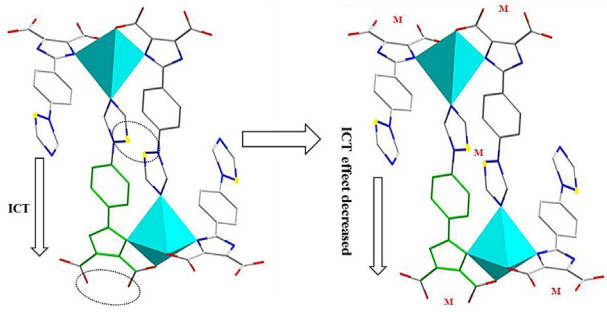

Figure 10. (Colour online) Luminescence sensing effect of **1–3** induced by the decrease of ICT, which may be due to the coordination of Fe^{3+} or K^+ with organic ligands.

of various metal ions on the surface of **1–3**, in our opinion, hardly affects their structures.

In this paper, to illuminate the weakening luminescent intensity or shift of emission peak position, ICT should be incorporated to translate analyte binding into a spectroscopic signal change (*34–37*). The metal cations introduced, Fe^{3+} or K^+, may interact with the uncoordinated atoms, oxygen and nitrogen atoms of the organic linkers, and may abate the corresponding ICT effect. Thus, we suspect this kind of fluorogenic probes for metal ions (Fe^{3+} or K^+) is developed by virtue of their strong coordinating abilities with electronegative heteroatoms (N, O, etc.) to decrease the ICT effect (Figure 10).

4. Conclusion

In summary, three luminescent Zn(II) and Cd(II) MOFs based on two kinds of novel semi-rigid ligands, *p*-IPh-H_3IDand *p*-TIPhH_3ID, have been successfully synthesised under solvothermal conditions. The selectivity and sensitivity of the fluorescence response of **1–3** to Fe^{3+} and K^+ show that they could be used as fluorescence sensors for Fe^{3+} and K^+. Moreover, further study and speculation of the mechanism illustrate that the majority of the luminescent response to different ions can result from the interaction of metal ions with the imidazole dicarboxylate ligands, and thus affect the ICT efficiency. It is to be expected that more related microporous Zn or Cd MOFs will need to be prepared to explore their sensing properties.

Disclosure statement

No potential conflict of interest was reported by the authors.

Funding

The authors gratefully acknowledge the financial support by the National Natural Science Foundation of China [grant number 21571156], [grant number J1210060]; Henan Province Foundation and Advanced Technology Research Project [Project number 162300410206].

References

(1) Eddaoudi, M.; Sava, D.F.; Eubank, J.F.; Adil, K.; Guillerm, V. *Chem. Soc. Rev.* **2015**, *44*, 228–249.
(2) Zhu, Q.-L.; Xu, Q. *Chem. Soc. Rev.* **2014**, *43*, 5468–5512.
(3) Kole, G.K.; Vittal, J.J. *Chem. Soc. Rev.* **2013**, *42*, 1755–1775.
(4) Zhou, H.-C.; Long, J.R.; Yaghi, O.M. *Chem. Rev.* **2012**, *112*, 673–674.
(5) Stock, N.; Biswas, S. *Chem. Rev.* **2012**, *112*, 933–969.
(6) Amo-Ochoa, P.; Felix, Z. *Coord. Chem. Rev.* **2014**, *276*, 34–58.
(7) Getman, R.B.; Bae, Y.-S.; Wilmer, C.E.; Snurr, R.Q.R. *Chem. Rev.* **2012**, *112*, 703–723.
(8) Liu, J.W.; Chen, L.F.; Cui, H.; Zhang, J.Y.; Zhang, L.; Su, C.Y. *Chem. Soc. Rev.* **2014**, *43*, 6011–6061.
(9) Horiuchi, S.; Kumai, R.; Tokura, Y. *J. Am. Chem. Soc.* **2013**, *135*, 4492–4500.
(10) Nagarkar, S.S.; Desai, A.V.; Ghosh, S.K. *Chem. Asian J.* **2014**, *9*, 2358–2376.
(11) Wang, C.; Liu, D.M.; Lin, W.B. *J. Am. Chem. Soc.* **2013**, *135*, 13222–13234.
(12) Kreno, L.E.; Leong, K.; Farha, O.K.; Allendorf, M.; Duyne, R.P.V.; Hupp, J.T. *Chem. Rev.* **2012**, *112*, 1105–1125.
(13) Feng, X.; Zhou, L.I.; Wang, L.Y.; Zhou, J.G.; Shi, Z.Q.; Shang, J.J. *Inorg. Chim. Acta* **2013**, *394*, 696–702.
(14) Zhai, Q.G.; Zeng, R.R.; Li, S.N.; Jiang, Y.C.; Hu, M.C. *Cryst. Eng. Commun.* **2013**, *15*, 965–976.
(15) Li, Z.F.; Luo, X.B.; Gao, Y.C.; Lu, H.J.; Li, G. *Inorg. Chim. Acta* **2012**, *384*, 352–362.
(16) Xiong, Z.F.; Gao, R.M.; Xie, Z.K.; Guo, B.B.; Li, L.; Zhu, Y.Y.; Li, G. *Dalton Trans.* **2013**, *42*, 4613–4624.
(17) Wang, W.Y.; Niu, X.L.; Gao, Y.C.; Zhu, Y.Y.; Li, G.; Lu, H.J.; Tang, M.S. *Cryst. Growth Des.* **2010**, *10*, 4050–4059.
(18) Zhang, Y.; Luo, X.B.; Yang, Z.L.; Li, G. *Cryst. Eng. Commun.* **2012**, *14*, 7382–7397.
(19) Guo, M.W.; Chen, N.; Yue, Z.F.; Zhang, Y.; Li, G. *Cryst. Eng. Commun.* **2012**, *14*, 4955–4958.
(20) Zhang, Y.; Guo, B.B.; Li, L.; Liu, S.F.; Li, G. *Cryst. Growth Des.* **2013**, *13*, 367–376.
(21) Guo, B.B.; Li, L.; Wang, Y.; Zhu, Y.Y.; Li, G. *Dalton Trans.* **2013**, *42*, 14268–14280.
(22) Li, L.; Guo, B.B.; Zhang, J.; Li, G. *Inorg. Chem. Commun.* **2013**, *36*, 86–89.
(23) Zheng, Y.H.; Tan, C.L.; Wang, Q.M.; Zhang, C.C. *Solid State Sci.* **2011**, *13*, 1687–1691.
(24) Das, S.; Saha, D.; Bhaumik, C.; Dutta, S.; Baitalik, S. *Dalton Trans.* **2010**, *39*, 17–20.
(25) (a) Cai, S.L.; Zheng, S.R.; Fan, J.; Xiao, T.T.; Tan, J.B.; Zhang, W.G. *Inorg. Chem. Commun.* **2011**, *14*, 937–939; (b) Yue, Z.F.; Chen, Z.N.; Yao, M.J.; Wang, H.L.; Li, G. *RSC Adv.* **2014**, *4*, 33537–33540.
(26) Lebedev, A.V.; Lebedeva, A.B.; Sheludyakov, V.D.; Kovaleva, E.A.; Ustinova, O.L.; Shatunov, V.V. *Russ. J. Gen. Chem.* **2007**, *77*, 949–953.
(27) Shelddrick, G.M. *SHELX-97, Program for the Solution and Refinement of Crystal Structures*, University of Göttingen: Germany; **1997**.

(28) Croitor, L.; Coropceanu, E.B.; Masunov, A.E.; Rivera-Jacquez, H.J.; Siminel, A.V.; Zelentsov, V.I.; Datsko, T.Y.; Fonari, M.S. *Cryst. Growth Des.* **2014**, *14*, 3935–3948.
(29) Pointillart, F.; Jung, J.; Berraud-Pache, R.; Le Guennic, B.; Dorcet, V.; Golhen, S.; Cador, M.O.; Guyot, Y.; Decurtins, S.; Liu, S.-X.; Ouahab, L.. *Inorg. Chem.* **2015**, *54*, 5384–5397.
(30) Zheng, M.; Tan, H.Q.; Xie, Z.G.; Zhang, L.G.; Jing, X.B.; Sun, Z.C. *Appl. Mater. Interfaces* **2013**, *5*, 1078–1083.
(31) Chen, B.L.; Wang, L.B.; Xiao, Y.Q.; Fronczek, F.R.; Xue, M.; Cui, Y.J.; Qian, G.D. *Angew. Chem. Int. Ed.* **2009**, *48*, 500–503.
(32) Cui, J.S.; Wong, Y.L.; Zeller, M.; Hunter, A.D.; Xu, Z.T. *Angew. Chem. Int. Ed.* **2014**, *53*, 14438–14442.
(33) Zhou, Y.; Zhang, J.F.; Yoon, J.Y. *Chem. Rev.* **2014**, *114*, 5511–5571.
(34) Haugland, R.P. *The Handbook: A Guide to Fluorescent Probes and Labelling Technologies*10th ed.; Molecular Probes: Eugene, OR, 2005.
(35) Grynkiewicz, M.P.; Tsien, R.Y. *Biol. Chem.* **1985**, *260*, 3440–3450.
(36) Tsien, R.W.; Lipscombe, D.; Madison, D.V. *Trends Neurosci.* **1988**, *11*, 431–438.
(37) Callan, J.F.; de Silva, A.P.; Magri, D.C. *Tetrahedron* **2005**, *61*, 8551–8588.